

Between all possible accelerometer configurations, the quad bridge¹ structure allows a seismic mass flat movement accelerometer and it matches with the vertical movement of the bridges. As can be seen in fig. 2.17, seismic mass is connected to the frame via the bridges located near the vertex. The mechanical stress on the bridges is given by [17]

$$T(x) = \frac{3F\left(\frac{a_1}{2} - x\right)}{b_1 h_1^2} \quad (2.16)$$

where F is the force that the acceleration causes to the seismic mass, x is the position considering the origin to be located in the frame and the rest of the parameters are defined in fig. 2.17.

From eq. (2.16), it can be seen that maximum stress is produced at x=0 and x=a₁, corresponding to the bridge's edges, being its value

$$T(x = 0, a_1) = \pm \frac{3Fa_1}{2b_1 h_1^2} \quad (2.17)$$

When this magnitude is higher than 6-9 GPa, the accelerometer bridges suffer from so high mechanical stress that could cause the structure to crack.

Natural frequency can also be known by ways of the Rayleigh method, which gives,

$$\omega_n = \frac{1}{2\pi} \sqrt{\frac{2Yb_1 h_1^3}{ma_1^3}} \quad (2.18)$$

where Y stands for the silicon Young modulus. As compared to other accelerometer configurations, as could be the more widely employed cantilever bridges [17] (where the mass is fixed to the frame only by one side), the quad bridge structure generally has a much higher natural frequency for its lowest vibrational mode. Thus, this design its advantageous for those applications that would require a wider bandwidth.

¹ It has to be noted that the term *bridge* is not the most commonly employed in MEMS, but is *beam*. However, in order to distinguish between the mechanical part and the *light beam*, *bridge* will be used throughout this work.

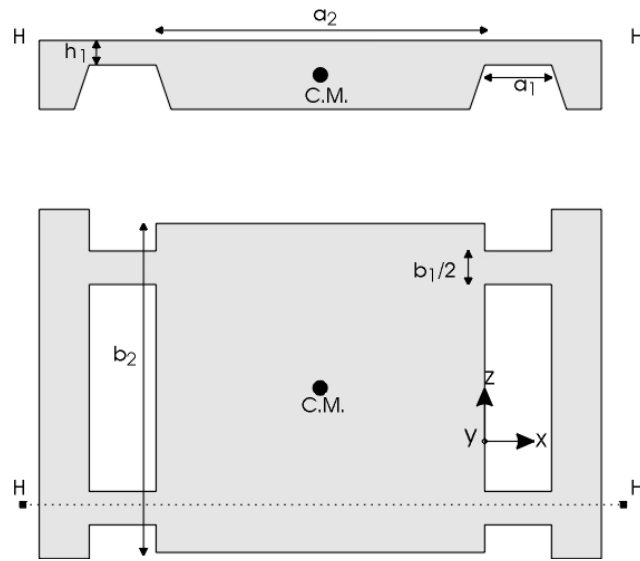
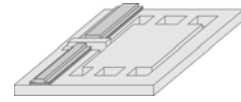
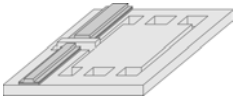


Fig 2.17.: Quad bridge standard geometry.

Two different factors related to acceleration should be taken into account when designing accelerometers. Firstly, although the device is designed to detect speed variations in the y axis, by ways of the previously defined sensitivity, its output response could be affected by crossed accelerations, that is, displacements either in the x or z axis caused by speed variations in the y axis. This factor should be considered since it could provide with significant errors on the acceleration measurement. Due to the fact that the accelerometer center of gravity is not located at the same level as the bridge. Then, the so-called lateral 3D effect is also observed: when the structure suffers from acceleration in the direction of the bridges, a force momentum is produced that causes mass to be displaced, increasing the crossed accelerations. This latter effect is especially important in the cantilever bulk configuration [17]. On the other hand, quad-bridge accelerometer, due to its configuration, does not suffer from crossed acceleration in the direction orthogonal to the bridges, although in the parallel direction the crossed acceleration still prevails. Thence, quad-bridge accelerometer configuration, as compared to cantilever, should provide with more feasible results due to its lower crossed accelerations.

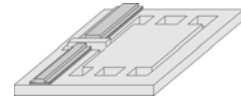
The transduction principle in accelerometers can be either based on mechanical strain or in mechanical stress variation. Those that belong to the first category measure the spring deformation that cause the displacement of some of its



components. Capacitive, resistive and optical accelerometers are its most significant examples. On the contrary, examples of accelerometers that change its features as a function of the mechanical stress variations could be resonant, piezjunction or piezoresistive.

To overcome the inherent problems of electrical-based accelerometers, as could be temperature dependence, low sensitivity and non stable output under electromagnetic interference (EMI) [18], there has been several proposals of optical-based accelerometers, both using integrated optics [19] and fiber optics [20]. The complete immunity against EMI and the possibility of having the light sources far from the device also makes them extremely useful in highly explosive atmospheres or where a strong electromagnetic field is present. Among the different configurations available, we have chosen two main actuation principles: if the FSZ is partially or completely blocked by an absorbent media, that is, if there exists a diaphragm that controls the light coupled to the output waveguide, we will refer to them as diaphragm optical accelerometers. If no absorbent media is placed on the FSZ, but the waveguides are somehow misaligned, we have labeled them as misalignment optical accelerometers.

Again, the question arises from the fact that up to date, the most common light guiding structures used on optical accelerometers have a high refractive index layer (frequently silicon nitride) in a cantilever configuration [20]. Although they could be considered as optimum for MOEMS applications (mainly due to its high confinement), it has to be noted that these waveguides normally have thicknesses around $0.2\mu\text{m}$. Although this dimension allows obtaining waveguides working in the visible range, the dimensions of the light source should also be taken into account: if end-fire coupling is used, then light is injected into the integrated optical device by ways of a single mode fiber optic, whose core has a diameter of $4\mu\text{m}$. The large difference between the relative areas of both structures causes an extremely high insertion losses ($>20\text{ dB}$). Moreover, in order to obtain cross-section light confinement, the core of integrated optical waveguides is partially etched, forming the so-called rib. In silicon nitride waveguides this rib seldom exceeds 5 nm in size, being impossible to see it at naked eye and hardening the alignment. Moreover, optical accelerometers should be able not only to detect when speed changes are produced, but also the magnitude of this change. If



waveguides with high numerical aperture are used (as is the case of silicon nitride), the lineal working range is quite small, reducing the device sensitivity. Hence, using ARROW configuration in uniaxial optical accelerometers offers several advantages: low insertion losses, injection easiness and wide lineal range.

The optical accelerometer configurations proposed result from the combination of two opposite technologies: integrated optics and MEMS. While the former demands for relatively thick layers so as to obtain good light confinement, the latter avoids to have multilayer structures, in order not to have the so-called bimetal effect, by which two material with different mechanical stresses or different thermal coefficients that cause structures to bend. Agreement has been achieved having only waveguides in very concrete accelerometer regions, far away from the weal mechanical parts (as could be the bridges).

2.3.1.2.1 Diaphragm Uniaxial Optical Accelerometers

The basic configuration of the diaphragm accelerometer proposed can be seen in fig. 2.18a. It consists of two ARROW-A waveguides of different width (14 μm for the input and 50 μm for the output) placed head-to-head. In the middle region, a diaphragm has been designed so as to absorb part of the light emitted from the input waveguide, as shown in fig 2.18b. Since this diaphragm is connected to a seismic mass, speed variation causes the mass and the diaphragm to move, causing a variation of the total amount of optical power at the output waveguide. It has to be considered that the diaphragm is made of silicon, which is absorbent at the working wavelength (633nm), hence, not only the diaphragm reflects part of the light, but also absorbs the fraction that its injected into it.

For the design of the optimum diaphragm thickness, the attenuation of a light beam with a wavelength of 633nm propagating through silicon should studied. As can be seen in fig. 2.19, for values above 6 μm , losses are so high that it could be considered that light is completely absorbed by the diaphragm. However, sometimes during the technological steps, there exists the possibility that some dimensions were reduced, especially if dry etching is used. For this reason, we have chosen a 20 μm wide diaphragm, which should be enough to overcome all possible problems during fabrication.

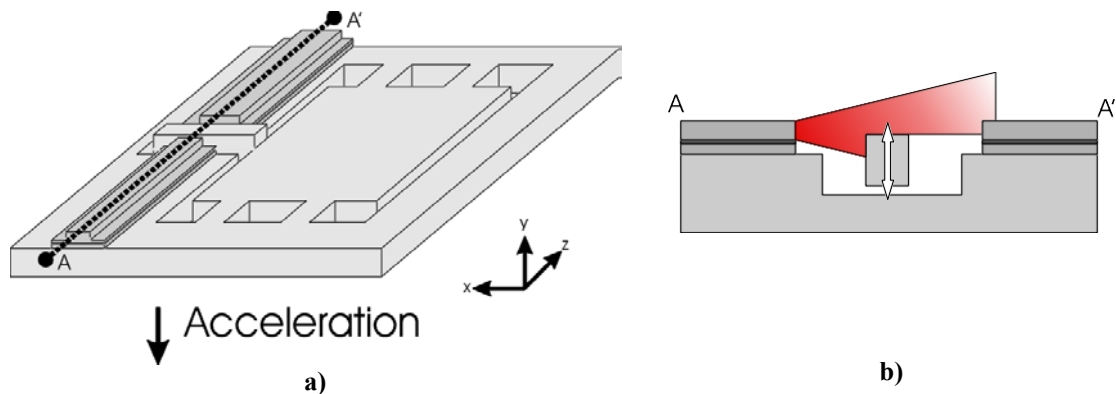
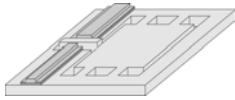


Fig 2.18.: a) Scheme of the diaphragm accelerometer proposed. b) AA' cut of fig 2.16a, where it can be seen both the input and the output waveguides, together with the diaphragm, which is the main responsible of the losses variation.

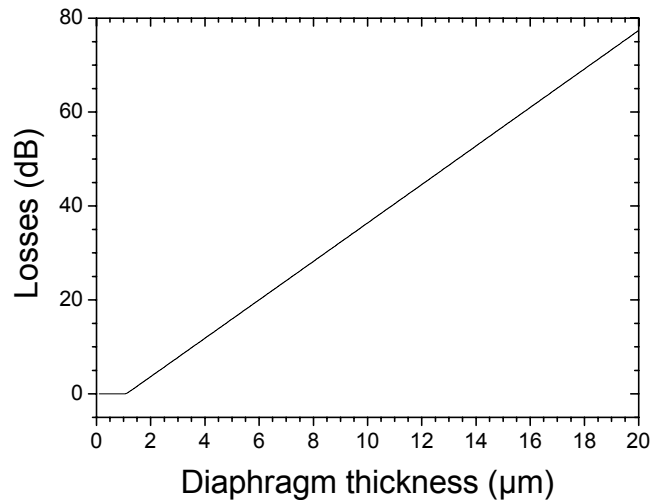
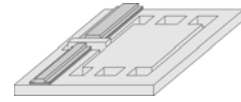


Fig 2.19.: Losses in a light beam with a wavelength of 633nm propagating through silicon.

2.3.1.2.2 Misalignment Uniaxial Optical Accelerometers

In the previous accelerometer design it was shown that in order to be able to detect acceleration not only in the $-y$ direction, but also in the y direction, at zero g 's the diaphragm should be placed at the center of the waveguide. Hence, the first step on the fabrication would be a surface etch. The correct behavior of the sensor strongly depends on this etch. A sub- or an overetching would cause an irreversible lost of the optimum measurement range. For misalignment sensors, no initial etching is needed in its fabrication. Thus, although it would not be possible to distinguish between positive and negative acceleration values, the misalignment uniaxial optical accelerometers are inherently self-aligned, which greatly simplifies its technology.



The scheme of the proposed accelerometer can be seen in fig. 2.20a. In this case, while the input and output are fixed on the frame, a third waveguide, called the sensing waveguide, is placed over the seismic mass. If there are no speed variations, all three waveguides are aligned and a maximum of power is obtained at the output, as shown in fig 2.20b. When an acceleration is produced, the seismic mass and straightforwardly, the sensing waveguide are displaced, causing a double misalignment (input-sensing and sensing-output) increasing the device losses. What would be desirable in this accelerometer would be that the mass displacement (i.e. the misalignment) to be proportional to the acceleration.

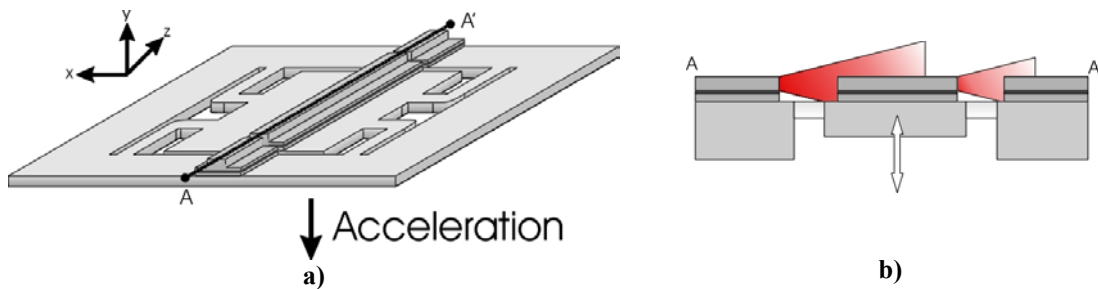
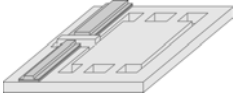


Fig 2.20.: a) Scheme of the misalign accelerometer proposed. b) AA' cut of fig 2.19a, where it can be seen the both the input and the output waveguides placed at the frame and the sensing waveguide on the seismic mass, which detects speed variations.

Thence, it would be extremely useful knowing which are the expected losses as a function of the waveguide misalignment, since the mechanical structure that held the sensitive waveguide yet is to be configured. There are, however, some points that the structure should fulfill: mass movement range should be as large as possible in order to have large power differences. In terms of sensitivity, at least 3dB/ μm should be obtained for accurate device characterization

When comparing the working range of ARROW and TIR waveguides with high Δn_{ce} (fig. 2.21a), it can be seen that the latter have much higher sensitivity (since small misalignments cause an huge power variation at the output). However, the linear region (2^{nd} derivative of the losses) where losses are directly proportional to acceleration changes (see figure 2.21b) is extremely small. Thence, optical accelerometers based on high Δn_{ce} waveguides mostly act as a switch. On the other hand, those based upon ARROW waveguides have a much larger working range, being



capable to measure acceleration changes with non-critical alignment and with low numerical aperture.

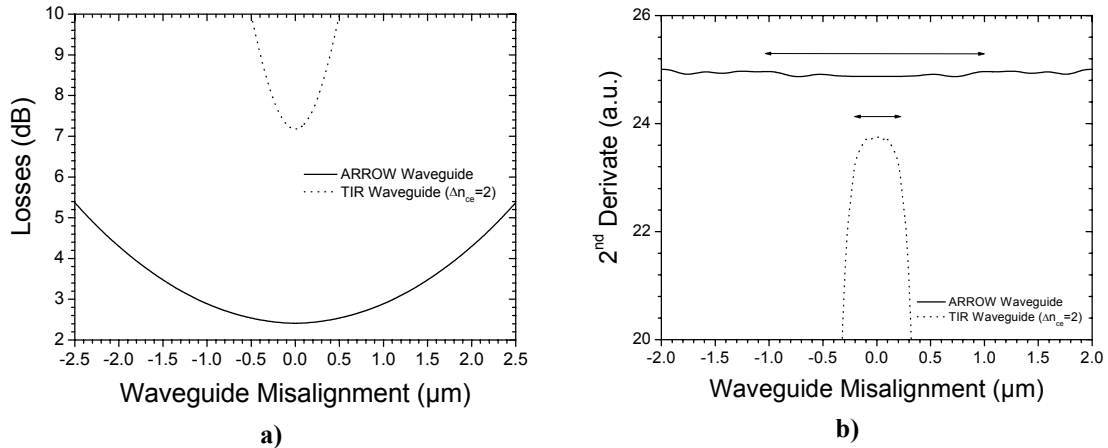


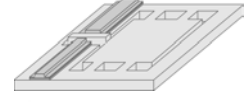
Fig 2.21.: a) Total losses due to waveguide misalignment in a quad bridge optical accelerometer with 300nm-thick TIR waveguide ($\Delta n_{ce}=2$) or ARROW waveguides. b) Linear regions where losses are directly proportional to misalignment. Waveguides were 30μm-distanced.

2.3.2 Phase Change-based Devices

Measurement by interferometry maybe is one of the most sensitive techniques employed, not only in integrated optics, but also in several other application fields. If light coming from a coherent source is split in two beams, and each one follows a slightly different optical path, when recombining them, an interference pattern is obtained due to the phase change between both beams, which provides information concerning the difference between the optical paths. This operation principle could be applied to any field, especially in sensors or quality control, since its high sensitivity allows detecting the slightest variation. Examples of devices based upon this operation principle are Mach-Zehnder interferometers or Multimode interference couplers.

2.3.2.1 Interferometric Devices I: Mach-Zehnder Interferometer (MZI)

Probably, the Mach-Zehnder configuration is the most well known interferometer in integrated optics. Its principle of operation is relatively simple, however extremely effective. It consists on an Y-divider headed to an Y-junction, as shown in fig. 2.22. Light entering through the input single mode waveguide splits into two beams, which have a relatively large distance so as not to interact between them.



After a given distance, light coming from both branches is recombined, via the Y-junction, so as to form a single signal. If the optical path on both branches is exactly equal, there will not be interference pattern at the output. On the contrary, if a perturbation is applied during a certain length L to one branch, a phase difference $\Delta\Phi$ between the light propagating through the two waveguides will be introduced. This fact leads to an intensity modulation at the device output, which can be written as:

$$I = \frac{I_0}{2} \left[E_{sens}^2 + E_{ref}^2 + 2E_{sens} E_{ref} \cos \Delta\Phi \right] \quad (2.19)$$

$$\Delta\Phi = \frac{2\pi L}{\lambda} \left[n_{eff,sens} - n_{eff,ref} \right] \quad (2.20)$$

Where E is the electric field propagating along the waveguide, n_{eff} is the effective refractive index and L is the sensor region. The labels *sens* and *ref* stands for the sensing and the reference arm, respectively.

The intensity at the output is a simple interference pattern caused by the sum of two slightly different waves. Following the principles of interferometric theory, it becomes essential that the contrast of this pattern to be the maximum available. Whether interference minimums and maximums could be distinguished or not depends on a factor called *fringe visibility* (v), which has the form:

$$v = \frac{(I_{max} - I_{min})}{(I_{max} + I_{min})} \quad (2.21)$$

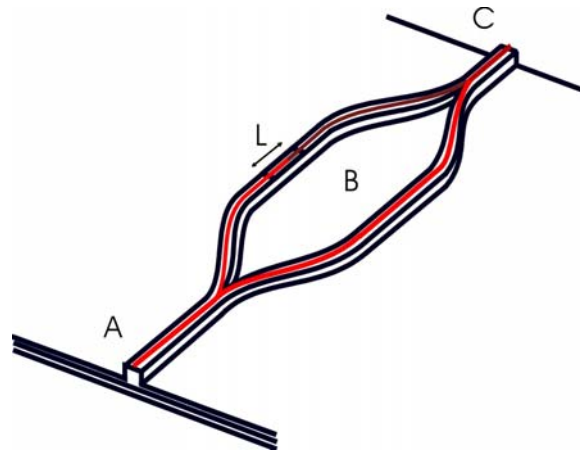
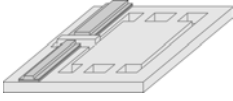


Fig 2.22.: Mach-Zehnder interferometer. Light injected in the input waveguide (A), is split in two branches (B). After varying the relative optical path during a length L , both are recombined again at (C).



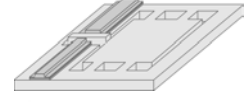
If a single light source is used, then $E_{sens}=(1-E_{ref})$, hence, the fringe visibility is:

$$v = \frac{E_{sens}(1-E_{sens})}{E_{sens}^2 + (1-E_{sens})^2} \quad (2.22)$$

It can be proved that maximum v values are obtained when $E_{sens}=1/2$, that is, optimum MZI reading is obtained when the splitting is exactly the same (3dB) at both branches. Although this division can be easily achieved in classical optics (using a beamsplitter) this is not so easy in integrated optics. So far, there are two main problems with integrated MZI: as it will be discussed in the next chapter, the precision and the size of the Y-junction edge depends on the technology used. Moreover, the angle between waveguides rarely has a value above 1° . Thence, waveguides slowly separates. Standard technology is unable to perform accurately this kind of edges and normally they become rounded when the distance between the waveguides is the same than the minimum dimension obtainable with the technology used. This rounding is uncontrollable and 3dB dividers are difficult to obtain in the form of an Y-junction. The second problem with MZI arises from its modal behavior. The previous analysis has been done considering a single mode on each branch, that is, considering that all waveguides in the MZI are single mode. If it is not so, intensity pattern at the output will not be defined by expression 2.20, since more field contributions should be considered. Hence, if waveguides have to be single-mode in the cross section, ribs have to be as minimum as possible so as to avoid several modes in the horizontal direction (in the vertical axis of an ARROW-based MZI, vertical modes higher than TE_0 are filtered out due to their excessive losses). However, as the rib decreases, the confinement is worse and losses at the Y-junctions dramatically increase. Thence, it will become necessary to reach an agreement between the confinement factor and the modal properties of the MZI waveguides.

2.3.2.2 Interferometric Devices II: Multimode Interference Couplers (MMI)

Multimode interference couplers are based on self-imaging principles [21]. Self imaging is defined as the property that multimode waveguides have by which an arbitrary input field profile is reproduced in single or multiple images at periodic intervals along the propagation axis. As can be seen in fig. 2.23, the MMI central structure is a highly multimode waveguide with effective refractive index, width and



length $n_{\text{eff},c}$, W_m and L_c , respectively. To inject light into and recover it from the multimode region, a certain number of single-mode waveguides are placed at both sides of this region. Such devices are normally referred as $N \times M$ MMI couplers, where N and M stands for the number of input and output waveguides, respectively.

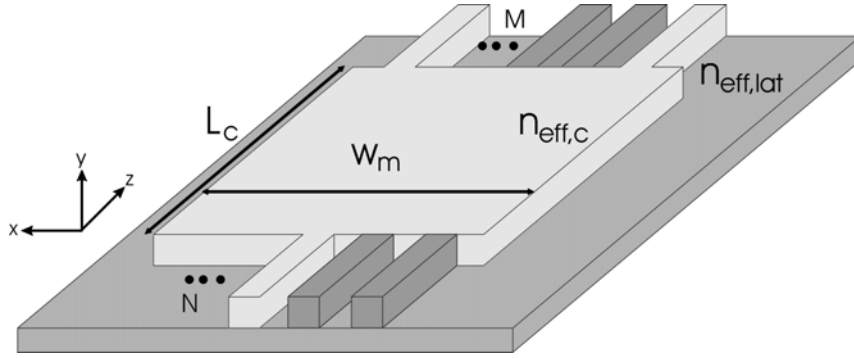


Fig 2.23.: Schematic structure of a multimode interference coupler (MMI) with N inputs and M outputs.

In order to understand how a MMI works, it is necessary to study the multimode region properties. Depending on its width W_m , it will have a larger number of modes ($m=0, 1, \dots, p-1$), as presented in fig. 2.24. By simple deduction from Maxwell equations [10], the wavenumber in the y direction ($k_{y,g}$), the propagation constant β_m of each mode m and the effective refractive index $n_{\text{eff},c}$ is given by:

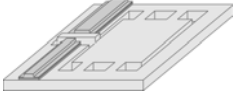
$$k_{y,m}^2 + \beta_m^2 = \frac{2\pi}{\lambda} n_{\text{eff},c}^2 \quad (2.23)$$

with

$$k_{y,m} = \frac{(m+1)\pi}{W_{e,m}} \quad (2.24)$$

where the real multimode waveguide width has been replaced by an effective amplitude $W_{e,m}$ that takes into account the different penetration that each mode has at the lateral boundaries, associated to the polarization-dependent Goos-Hänchen shift. Hence, there exists an effective width for each mode. However, it is approximated by these of the lowest mode W_{e0} (W_e for simplicity), which has the form:

$$W_{e,m} \approx W_e = W_m + \left(\frac{\lambda}{\pi} \right) \left(\frac{n_{\text{eff},c}}{n_{\text{eff},lat}} \right)^{2\sigma} \frac{1}{\sqrt{n_{\text{eff},c}^2 - n_{\text{eff},lat}^2}} \quad (2.25)$$



Where $\sigma=0$ for TE and $\sigma=1$ for TM polarizations. If waveguides are highly confining, the penetration depth is negligible and $W_e \approx W_m$. It also can be shown that the propagation constant β_m is

$$\beta_m \approx \frac{2\pi}{\lambda} n_{eff,c} - \frac{(m+1)^2 \pi \lambda}{4 n_{eff,c} W_e^2} \quad (2.26)$$

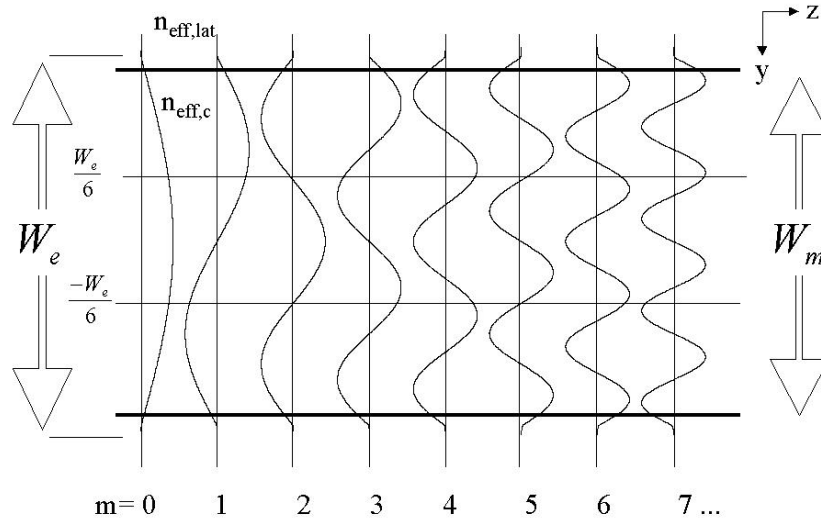


Fig 2.24.: Lateral field profiles corresponding to the first 8 modes of a MMI with width W_m and effective width (if the Goos-Hänchen effect is considered) W_e .

At this point, L_π can be defined as the beat length for the two lowest order modes as

$$L_\pi = \frac{\pi}{\beta_0 - \beta_1} \approx \frac{4}{3} \frac{n_{eff,c} W_e^2}{\lambda} \quad (2.27)$$

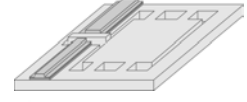
Thence, the propagation constant difference can be written as:

$$(\beta_0 - \beta_m) = \frac{m(m+2)\pi}{\lambda 3 L_\pi} \quad (2.28)$$

If an input field $\Psi(y,0)$ is introduced at $z=0$ in the multimode waveguide, as shown in fig. 2.25, it will be decomposed as a sum of all waveguide guided modes

$$\Psi(y, z) = \sum_{m=0}^{p-1} c_m \psi_m(y) \exp[i(\omega t - \beta_m z)] \quad (2.29)$$

where ψ_m are the modal field distributions and c_m the field excitation coefficients that can be estimated by means of the overlap integrals



$$c_m = \frac{\int \Psi(y,0)\psi_m(y)dy}{\sqrt{\int \psi_m^2(y)dy}} \quad (2.30)$$

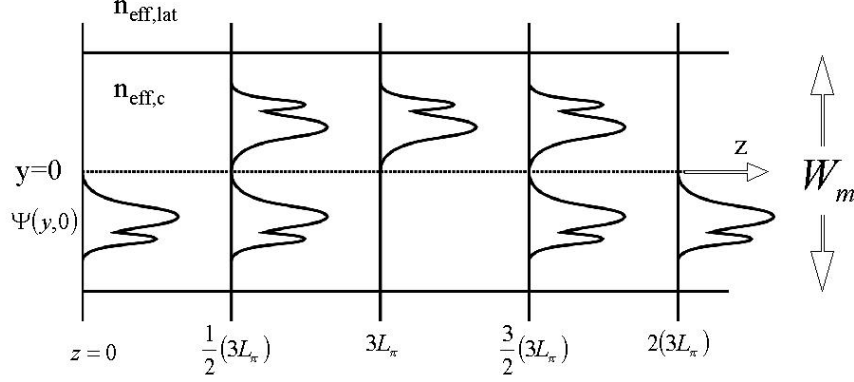


Fig 2.25.: Top-view multimode waveguide drawing where it can be observed the input field $\Psi(y,0)$, a mirrored self-image at $(2s+1)L_\pi$, a direct self-image at $(2s)L_\pi$, and two-fold images at $(2s+1)/2L_\pi$.

If all phases are written as a function of these of the fundamental mode and assuming the temporal dependence implicit thereafter, eq. (2.29) can be rewritten as

$$\Psi(y, z) = \sum_{m=0}^{p-1} c_m \psi_m(y) \exp[i(\beta_0 - \beta_m z)] \quad (2.31)$$

Using eq. (2.28) it is found that at a certain distance L , the field profile is given by

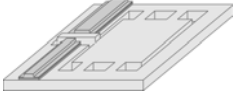
$$\Psi(y, L) = \sum_{m=0}^{p-1} c_m \psi_m(y) \exp\left[i\left(\frac{m(m+2)\pi}{3L_\pi}\right)\right] \quad (2.32)$$

It can be observed under certain circumstances, the field profile at a distance L will be an exact reproduction (self-imaging) of the initial field. It is possible to distinguish between *General Interference* when the excitation is independent of the modal field properties and *Restricted Interference* when only a part of the waveguide modes are excited.

From eq. (2.32), it is obvious that $\Psi(y,0)=\Psi(y,L)$ if

$$\exp\left[i\left(\frac{m(m+2)\pi}{3L_\pi}\right)\right] = 1 \quad \text{or} \quad (-1)^m \quad (2.33)$$

The first equation means that all the phase changes after a distance L must differ by integer multiples of 2π . Hence, all the modes interfere with the same relative phases as if they were at $z=0$. The image observed is a direct replica of the input field. The second



expression states that phase changes must be even and odd multiples of π , being the odd and the even modes in antiphase. If it is taken into account that

$$\psi_m(-y) = \begin{cases} \psi_m(y) & \text{for } m \text{ even} \\ -\psi_m(y) & \text{for } m \text{ odd} \end{cases} \quad (2.34)$$

the self-images will be alternatively mirrored with respect to the symmetry plane $y=0$.

Considering

$$m(m+2) = \begin{cases} \text{even} & \text{if } m \text{ even} \\ \text{odd} & \text{if } m \text{ odd} \end{cases} \quad (2.35)$$

It can be seen that the first conditions at eq. (2.33) will be satisfied if

$$L_c = g(3L_\pi) \quad \text{with } g = 0,1,2,\dots \quad (2.36)$$

for g even and g odd, respectively. The presence of this factor g means that in MMI couplers, there always exists the self-imaging periodicity. Hence, direct and mirrored images of the input field will be successively obtained at even and odd multiples of $3L_\pi$, respectively.

Previous results can be generalized so as to obtain expressions for M -fold images, obtained at intermediate positions. It can be proved [22] that a M -folded self-image can be obtained, in the general interference regime at length values given by

$$L_c = \frac{g}{M}(3L_\pi) \quad (2.37)$$

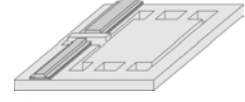
only if there exist no common divisor between g and M . At these values the field will be of the form:

$$\Psi(y, L_\pi) = \frac{1}{C} \sum_{q=0}^{m-1} \Psi_{in}(y - y_q) \exp(i\varphi_q) \quad (2.38)$$

where C is a complex normalization constant with $|C| = M^{1/2}$, q refers to each of the M images along the y axis. $\Psi_{in}(y)$ is a development in a Fourier series of the input field $\Psi(y,0)$ with expression

$$\Psi_{in}(y) = \sum_{m=-\infty}^{\infty} [\Psi(y - 2mW_e, 0) - \Psi(-y + 2mW_e, 0)] \quad (2.39)$$

y_q and φ_q are given by



$$y_q = g(2q - M) \frac{W_e}{M} \quad (2.40)$$

$$\varphi_q = g(M - q) \frac{q\pi}{M} \quad (2.41)$$

Previous expressions allows confirming that at distances $z=L_\pi$, M images are obtained of the extended field $\Psi_{in}(y)$, located at $y=y_q$, with amplitude $M^{-1/2}$ and phase φ_q . In turn, it leads to obtaining M images of the input field $\Psi(y,0)$.

So far, no condition on the exciting has been applied. However, it could have been noted that there exists some y values where some modes have a minimum and will not be excited if the modal excitation was placed there, causing a significant reduction of the modes involved in the self-imaging process and thenceforward, a total length reduction.

If input waveguides are placed at $\pm W_e/6$, modes $m=2,5,8,\dots$ have a zero amplitude at this point and will not be excited. Their overlap integrals between the symmetric input field (typically a gaussian beam) and the asymmetric mode will vanish and thence $c_m=0$ for $m=2,5,8,\dots$

Under this configuration, the modes contributing to the interference are paired, that is, $2m-(2m+1)$ modes have similar relative properties within its phase. This configuration will be therefore called *paired interference* and obviously in this case the number of input waveguides will be limited to two. Under *paired interference*, M-folded images are obtained at lengths [23]:

$$L_c = \frac{g}{M} (L_\pi) \quad (2.42)$$

If only one input waveguide is placed at $y=0$ (working under 1xM configuration), restricted interference can also be obtained. In this case, however, it can be seen that all odd order modes are not excited. That is, the overlap integral vanishes for all odd modes. Hence, the final imaging profile is obtained via the contribution of all even modes in the so-called *symmetric interference*. Under this restricted self-imaging configuration, M-folded images are obtained at

$$L_c = \frac{g}{M} \left(\frac{3L_\pi}{4} \right) \quad (2.43)$$

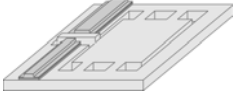


Table 2.3 summarizes the previously obtained results.

Interference on multimode region	General	Restricted	Paired
Inputs x Outputs	NXM	2XM	1XM
Image	$3L_\pi$	L_π	$3L_\pi/4$
M-folded image	$3L_\pi/M$	L_π/M	$3L_\pi/(4M)$
Modes unexcited ($c_m=0$)	None	$m = 2,5,8,\dots$	$m = 1,3,5,\dots$
Injected beams position	Any	$y = \pm W_e/6$	$y = 0$

Table 2.3: Summary of the properties of the general restricted and paired MMI devices.

Finally, the MMI fabrication tolerances for all its dimensions can be calculated. If each self-image at $z=L$ is considered as a gaussian beam, then, the loss penalty caused by a small variation of the total length δL can be evaluated by overlapping the defocused beam with the output waveguide field profile. 0.5dB losses are obtained when [24]:

$$\delta L \approx \frac{\pi n_{eff,c} w_0^2}{4\lambda} \quad (2.44)$$

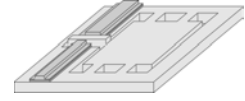
Where w_0 is the gaussian beam waist. It is noteworthy mentioning that length tolerance does not depend on the multimode waveguide dimensions. Hence, for a given wavelength and refractive index, the tolerance can be enhanced by wider input waveguides. The rest of the parameters can be directly related to the previous expression using eq. 2.27 and 2.36, which provide

$$\frac{\delta L}{L} = 2 \frac{\delta W_e}{W_e} = \frac{|\delta \lambda|}{\lambda} = \frac{\delta n_{eff,c}}{n_{eff,c}} \quad (2.45)$$

Thence, it is clear that MMI region should be made as short as possible in order to obtain more relaxed conditions for the rest of the parameters.

2.3.3 Evanescent Field Devices

Evanescent field maybe is the one of the most unknown light properties in confined media. However, it has several applications in telecommunications field: two or more waveguides placed closer each other are able to interchange periodically the optical power that they transmit. The distance that the waveguides have to be parallel so



as to transfer all the power depends on the working wavelength and morphology. From this operation principle, filters and multiplexers have been designed on the basis of evanescent field coupling.

At the beginning of this chapter, when single waveguides were studied, it was observed how any guided mode has an evanescent tail that propagates off from the core. If a second waveguide is closely placed so as to overlap the evanescent field of the modes propagating by both waveguides, a coupling between them will be produced. If light is injected to one of the waveguides, a periodic interchange of power between both waveguides will be obtained. Moreover, if the waveguides are identical, there will be a complete power transfer. These structures are called directional couplers. An scheme of which is presented in fig. 2.26.

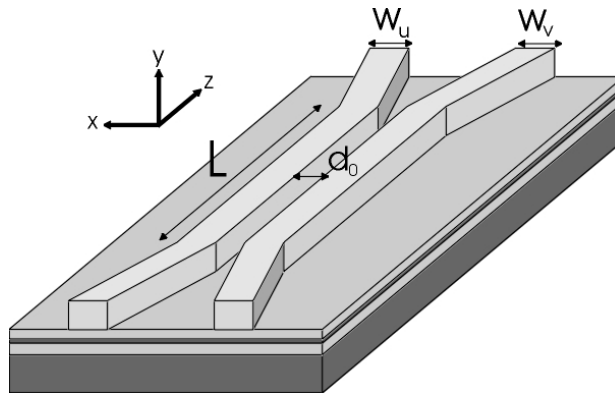
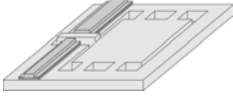


Fig 2.26.: Directional coupler in which two single-mode waveguides (u and v) with width W_u and W_v are parallel over a length L with a distance of d_0 between them.

Under the supposition of weakly interacting fields and single-mode waveguides, the coupled-mode theory [25] can be applied, obtaining the expressions for the field evolution along z ,

$$\begin{aligned} \frac{d\Psi_u(z)}{dz} &= -i\beta_u \Psi_u(z) - i\kappa_{uv} \Psi_v(z) \\ \frac{d\Psi_v(z)}{dz} &= -i\beta_v \Psi_v(z) - i\kappa_{vu} \Psi_u(z) \end{aligned} \quad (2.46)$$

where Ψ_u and Ψ_v are the field amplitudes at the directional coupler waveguides, being β_u and β_v their propagation constants. κ_{uv} and κ_{vu} represent the strength of the



interaction between the evanescent tails of the two modes and are referred to as coupling constants. If waveguides are independent, i.e, they do no interact, $\kappa_{uv} = \kappa_{vu} = 0$ and solutions of eq. (2.46) are of the form $\exp(-i\beta z)$, which is a non-perturbed single propagating wave.

As the coupling constant depends on the evanescent field overlap, it should be a function of the mode confinement inside the waveguide (which, in turn, is a function of the waveguide width and the rib etch), the separation between waveguides and the working wavelength. It can be shown [26] that it has the form:

$$\kappa_{s,t} = \frac{k^2}{2\beta_s} \frac{\int \int_{-\infty}^{+\infty} \Psi_s^* \Delta n_s^2 \Psi_t dx dy}{\int \int_{-\infty}^{+\infty} \Psi_s^* \Psi_s dx dy} \quad s, t = u, v \quad (2.47)$$

$$\Delta n_s^2 = n^2(x, y) - n_s^2(x, y) \quad s, t = u, v \quad (2.48)$$

where $n(x,y)$ and $n_s(x,y)$ are defined in fig. 2.27

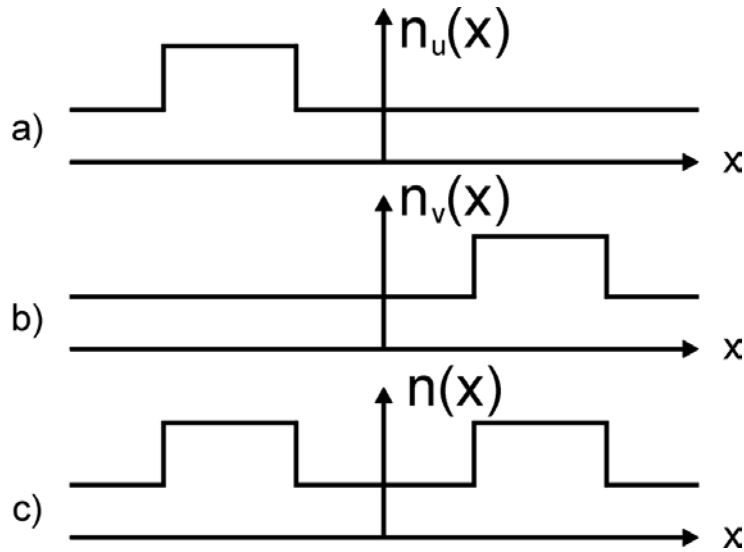
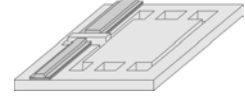


Fig 2.27.: a) and b) are the refractive index profiles of two isolated rib waveguides and c) is the refractive index profile of a parallel directional coupler.

Obviously, for parallel identical waveguides $\kappa_{uv} = \kappa_{vu} = \kappa$

Solving eq. (2.46), it can be seen that if at $z=0$ the fundamental mode in waveguide u is excited using a given field amplitude δ , while a different fraction α



allows exciting the fundamental mode of waveguide v , the power as a function of the propagation distance has the form:

$$|\Psi_u(z)|^2 = \alpha^2 \left[\frac{\kappa^2 \operatorname{sen}^2 \left(\sqrt{\frac{\Delta\beta^2}{4} + \kappa^2 z} \right)}{\frac{\Delta\beta^2}{4} + \kappa^2} \right] + \delta^2 \left[1 - \frac{\kappa^2 \operatorname{sen}^2 \left(\sqrt{\frac{\Delta\beta^2}{4} + \kappa^2 z} \right)}{\frac{\Delta\beta^2}{4} + \kappa^2} \right] - \alpha\delta \left[\frac{\kappa\Delta\beta \operatorname{sen}^2 \left(\sqrt{\frac{\Delta\beta^2}{4} + \kappa^2 z} \right)}{\frac{\Delta\beta^2}{4} + \kappa^2} \right] \quad (2.49)$$

where $\Delta\beta = \beta_u - \beta_v$. If there exist no losses in the directional coupler,

$$|\Psi_u(z)|^2 + |\Psi_v(z)|^2 = 1 \quad (2.50)$$

Under the standard excitation conditions, where a power unity is injected in waveguide u and there is no power in waveguide v (that is, $\delta=0$, $\alpha=1$) eq. (2.49) is simplified to

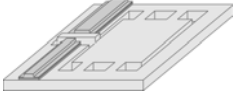
$$|\Psi_u(z)|^2 = \frac{\kappa^2 \operatorname{sen}^2 \left(\sqrt{\frac{\Delta\beta^2}{4} + \kappa^2 z} \right)}{\frac{\Delta\beta^2}{4} + \kappa^2} \quad (2.51)$$

As it can be seen, there exists a periodical power exchange as a function of the propagation distance, with period

$$T = \frac{\pi}{\sqrt{\frac{\Delta\beta^2}{4} + \kappa^2}} \quad (2.52)$$

The distance L_{c0} , defined as

$$L_{c0} = \frac{T}{2} = \frac{\pi}{2\sqrt{\frac{\Delta\beta^2}{4} + \kappa^2}} \quad (2.53)$$



is called the coupling length and corresponds to the distance required so as to have maximum power transfer between both waveguides. It also can be seen that the maximum intensity transferred is given by

$$|\Psi_v(z)|_{max}^2 = \frac{\kappa^2}{\frac{\Delta\beta^2}{4} + \kappa^2} \quad (2.54)$$

Only complete power transference between waveguides can take place when $\Delta\beta=0$, that is, having the two waveguides exactly the same propagation constant. In this situation, the coupling length will be given by

$$L_{c0}^{\Delta\beta=0} = \frac{\pi}{\beta_{sim} - \beta_{ass}} \quad (2.55)$$

where β_{sim} and β_{ass} are the symmetrical and asymmetrical modes of the overall structure and their values are given by

$$\beta_{sim,ass} = \frac{1}{2}(\beta_u + \beta_v) \pm \sqrt{\frac{1}{4}(\beta_u - \beta_v)^2 + \kappa^2} \quad (2.56)$$

Figure 2.28 shows the numerical evaluation of eq. (2.51). It can be observed how a slight variation of the propagation constant causes the variation of the coupling length value and forbids the complete power transfer between waveguides.

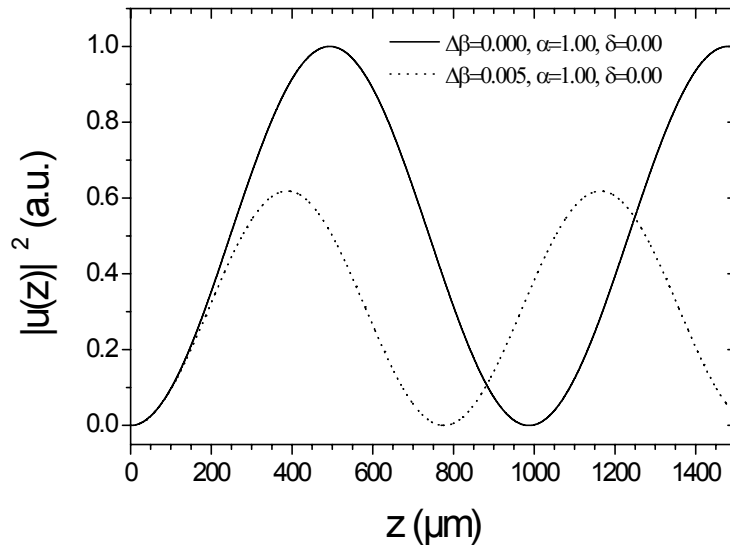
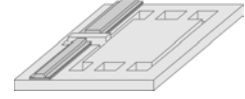


Fig 2.28.: Numerical evaluation of eq. (2.51) with $k=10^{-3}m^{-1}$ for identical and non-identical waveguide propagation constants.



If eq. (2.49) is studied, as shown in fig. 2.29, the behavior of the directional coupler can be modified through the simultaneous light injection in both waveguides. If the same power fraction is injected ($\delta=1$, $\alpha=1$) it can be observed how the periodical power transference is completely suppressed. Although previously we stated that if the propagation constants were different, only partial exchange of power could be obtained, this deduction was done considering injection on one waveguide only. As it also can be seen in fig 2.29, small variations on the propagation constants can be compensated by simultaneous light injection at both waveguides with balanced intensity. If the balance is broken, that is, if the light intensity in both waveguides is different, only partial transference of power is achieved.

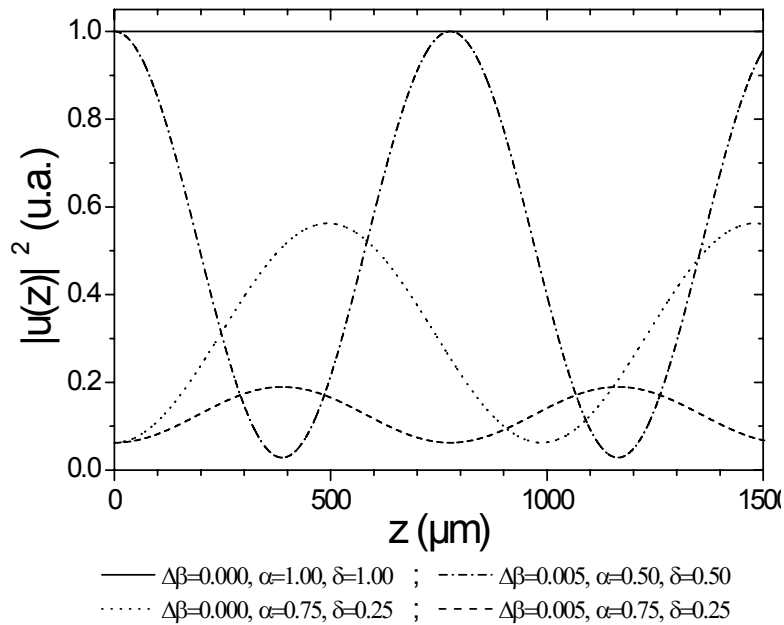
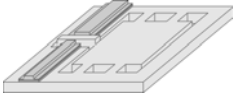


Fig 2.29.: Numerical evaluation of eq. (2.49) with $k=10^{-3}\text{m}^{-1}$ for identical and non-identical waveguide propagation constants and for balanced and unbalanced light excitation.

As an application example, directional couplers with identical waveguides can be used for the design of optical switches. If light is injected only in one waveguide and the parallel distance is the coupling length, the directional coupler it is said to be in the cross state (\otimes), because all the power injected from waveguide u is transferred to waveguide v . If a change in the propagation constants is introduced so as to vary the



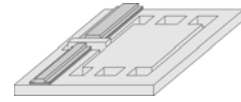
coupling length to $L_{c0}/2$, power will be no longer at v , but it will return to u , being now the directional coupler in the parallel state (\ominus). The minimum required propagation constant difference so as to change from cross state to parallel state is given by

$$\Delta\beta = \sqrt{\frac{3\pi}{L_{c0}}} \quad (2.57)$$

This change on the optical constants can be done using the electro-optic effect [27]. If a given oscillating voltage is applied, an oscillating value of $\Delta\beta$ will be obtained, causing the output signal modulation. It has to be noted, however, that this operation principle can only be applied to those compounds, such as lithium niobate or some III-V compounds where the electro-optical coefficient is extremely high. Unfortunately, this is not the case for silicon compounds. So, directional couplers based in silicon technology cannot be applied for electro-optical devices. However, the deep knowledge and the fabrication techniques in silicon make it very attractive for passive devices.

Bibliography

- [1] R.G.Hunsperger. *Theory of Optical Waveguides. Integrated Optics: Theory and Technology*. Springer-Verlag. 1995: 32-46.
- [2] M.A.Duguay, Y.Kokubun, T.L.Koch. *Antiresonant Reflecting Optical Waveguides in SiO₂-Si Multilayer Structures*. Appl.Phys.Lett. 49[1], 13-15. 1986.
- [3] T.Baba, Y.Kokubun. *New Polarization-Insensitive Antiresonant Reflecting Optical Waveguide (ARROW-B)*. IEEE Phot.Tech.Lett. 1[8], 232-234. 1989.
- [4] E.Hecht, A.Zajac. *La Propagación de la Luz. Optica*. Addison-Wesley. 1986: 64-99.
- [5] B.Saleh, M.Teich. *Resonator Optics. Fundamentals of Photonics*. 1991: 310-341.
- [6] T.Tamir. *Guided-Wave Optoelectronics*. Springer-Verlag. 1988: 1-50.
- [7] T.Baba, Y.Kokubun, T.Sakaki, K.Iga. *Loss Reduction of an ARROW Waveguide in Shorter Wavelength and its Stack Configuration*. J.Light.Tech. 6[9], 1440-1445. 1988.
- [8] E.A.Marcatili. *Dielectric Rectangular Waveguide and Directional Coupler for Integrated Optics*. Bell Syst.Tech.J. 48, 2071-2102. 1969.
- [9] R.M.Knox, P.P.Toulios. *Integrated Circuits for the Millimeter Optical Frequency Range*. Proc.Symp.Submillimeter Waves , 497-516. 1970.



- [10] A.K.Ghatak, K.Thyagarajan. *Electromagnetic Analysis of the Simplest Optical Waveguide*. *Optical Electronics*. Cambridge Univ. Press. 1989: 315-342.
- [11] P.P.Silvester, G.Pelosi. *Finite Elements for Wave Electromagnetics. Methods and Techniques*. IEEE Press. 1994.
- [12] C.M.Kim, R.V.Ramaswamy. *Modelling of Graded-Index Channel Waveguides Using Nonuniform Finite Difference Method*. *J.Light.Tech.* 7[10], 1581-1589. 1989.
- [13] Y.Chung, N.Dagli. *Analysis of Z-Invariant and Z-Variant Semiconductor Rib Waveguides by Explicit Finite Difference Beam Propagation Method with Nonuniform Mesh Configuration*. *IEEE J.Quant.Elect.* 27[10], 2296-2305. 1991.
- [14] Y.H.Chen, Y.T.Huang. *Coupling-Efficiency Analysis and Control of Dual Antiresonant Reflecting Optical Waveguides*. *J.Light.Tech.* 14[6], 1507-1513. 1996.
- [15] B.Saleh, M.Teich. *Beam Optics. Fundamentals of Photonics*. John Wiley & Sons, Inc. 1991: 80-106.
- [16] W.Göpel, J.Hesse, J.N.Zemel, E.Wagner, R.Dändliker, K.Spenner. *Sensors, a Comprehensive Survey. Volume 6: Optical Sensors*. VCH. 1991.
- [17] J.A.Plaza. *μAcelerómetros de Silicio. Chapter III*. Thesis. 1997. Universitat Autònoma de Barcelona.
- [18] N.Yazdi, F.Ayazi, K.Najafi. *Micromachined Inertial Sensors*. *Proced.IEEE* 86[8], 1640-1659. 1998.
- [19] J.M.López-Higuera, P.Mottier, A.Cobo, E.Ollier, M.A.Morante, C.Chabrol *et al.* *Optical Fiber and Integrated Optics Accelerometers for Real Time Vibration Monitoring in Harsh Environments: In-Lab and in-Field Characterization*. *Europ.Works.Opt.Fib.Sens.(SPIE)* 3483, 223-226. 1998.
- [20] J.Kalenik, R.Pajak. *A Cantilever Optical-fiber Accelerometer*. *Sens.& Act.A* 68, 350-355. 1998.
- [21] R.Ulrich, T.Kamiya. *Resolution of Self-Images in Planar Optical Waveguides*. *J.Opt.Soc.Am* 68[5], 583-592. 1978.
- [22] M.Bachmann, P.A.Besse, H.Melchior. *General Self-Imaging Properties in NxN Multimode Interference Couplers Including Phase Relations*. *Appl.Optics.* 33[18], 3905-3911. 1994.
- [23] L.B.Soldano, E.C.Pennings. *Optical Multi-Mode Interference Devices Based on Self-Imaging: Principles and Applications*. *J.Light.Tech.* 13[4], 615-627. 1995.
- [24] P.A.Besse, M.Bachmann, H.Melchior, L.B.Soldano, M.K.Smit. *Optical Bandwidth and Fabrication Tolerances of Multimode Interference Couplers*. *J.Light.Tech.* 12[6], 1004-1009. 1994.
- [25] K.Yasumoto. *Coupled-Mode Formulation of Parallel Dielectric Waveguides*. *Opt.Lett.* 18, 503-506. 1993.
- [26] H.Haus, W.P.Huang. *Coupled-Mode Theory*. *Proced.IEEE* 79[10], 1505-1518. 1991.
- [27] A.K.Ghatak, K.Thyagarajan. *Integrated Optics*. *Optical Electronics*. Cambridge Univ. Press. 1989: 421-460.